THE JOURNAL OF BIOLOGICAL CHEMISTRY VOL. 288, NO. 1, pp. 677–686, January 4, 2013

Mitoferrin-2-dependent Mitochondrial Iron Uptake Sensitizes Human Head and Neck Squamous Carcinoma Cells to Photodynamic Therapy*

Received for publication, September 25, 2012, and in revised form, November 5, 2012 Published, JBC Papers in Press, November 7, 2012, DOI 10.1074/jbc.M112.422667

Hsin-I Hung[‡§], Justin M. Schwartz[‡§], Eduardo N. Maldonado[‡§¶], John J. Lemasters[‡§¶‖], and Anna-Liisa Nieminen[‡§¶1]

From the [‡]Center for Cell Death, Injury, and Regeneration, Departments of [§]Drug Discovery and Biomedical Sciences and [‖]Biochemistry and Molecular Biology, and the [¶]Hollings Cancer Center, Medical University of South Carolina, Charleston, South Carolina 29425

Background: Here, we investigated whether iron mobilization enhanced photodynamic therapy (PDT)-induced cell killing.
Results: Lysosomal iron release and mitochondrial iron uptake through mitoferrin-2 (Mfrn2) acted synergistically to induce PDT-mediated and iron-dependent mitochondrial dysfunction and cell killing.
Conclusion: Mfrn2 plays a critical role in transporting iron to mitochondria to enhance PDT.
Significance: Head and neck cancers expressing higher Mfrn2 protein levels benefit more from PDT.

Photodynamic therapy (PDT) is a promising approach to treat head and neck cancer cells. Here, we investigated whether mitochondrial iron uptake through mitoferrin-2 (Mfrn2) enhanced PDT-induced cell killing. Three human head and neck squamous carcinoma cell lines (UMSCC1, UMSCC14A, and UMSCC22A) were exposed to light and Pc 4, a mitochondria-targeted photosensitizer. The three cell lines responded differently: UMSCC1 and UMSCC14A cells were more resistant, whereas UMSCC22A cells were more sensitive to Pc 4-PDT-induced cell death. In non-erythroid cells, Mfrn2 is an iron transporter in the mitochondrial inner membrane. PDT-sensitive cells expressed higher Mfrn2 mRNA and protein levels compared with PDT-resistant cells. High Mfrn2-expressing cells showed higher rates of mitochondrial Fe^{2+} uptake compared with low Mfrn2-expressing cells. Bafilomycin, an inhibitor of the vacuolar proton pump of lysosomes and endosomes that causes lysosomal iron release to the cytosol, enhanced PDT-induced cell killing of both resistant and sensitive cells. Iron chelators and the inhibitor of the mitochondrial Ca^{2+} (and Fe^{2+}) uniporter, Ru360, protected against PDT plus bafilomycin toxicity. Knockdown of Mfrn2 in UMSCC22A cells decreased the rate of mitochondrial Fe^{2+} uptake and delayed PDT plus bafilomycin-induced mitochondrial depolarization and cell killing. Taken together, the data suggest that lysosomal iron release and Mfrn2-dependent mitochondrial iron uptake act synergistically to induce PDT-mediated and iron-dependent mitochondrial dysfunction and subsequent cell killing. Furthermore, Mfrn2 represents a possible biomarker of sensitivity of head and neck cancers to cell killing after PDT.

Head and neck cancer, including cancers of the mouth, nose, oral cavity, and throat, is the sixth most common cancer worldwide (1). Current treatments for head and neck cancers include surgery, radiation, chemotherapy and any of these in combination (2). However, each of these treatments leads to undesirable side effects that cause systemic toxicity or disfigurement that can dramatically affect quality of life.

Photodynamic therapy (PDT)[2] is a localized treatment that uses a light-activated photosensitizer, which upon activation, transfers its high energy to oxygen and generates reactive oxygen species (ROS) that kill cancer cells. PDT is a non-invasive method, making it a promising alternative to conventional cancer therapy. PDT is best used for treatment of superficial cancerous lesions, including cutaneous neoplasms, head and neck cancers, and premalignant conditions such as Barrett esophagus (3, 4). These lesions are easily accessible to red laser light. Use of PDT in large solid tumors is more challenging. Depending on the wavelength of the photosensitizing light and the concentration of photosensitizer, the depth of tumor destruction ranges from a few mm to 1 cm. Decreased oxygen tension deep in poorly vascularized tumors can also result in decreased formation of singlet oxygen and other ROS, thereby diminishing the therapeutic effect of PDT. Thus, adjuvant treatments to increase intratumoral ROS production during PDT should increase treatment efficacy.

In our studies, we have used phthalocyanine 4 (Pc 4), which is a silicon phthalocyanine bearing a dimethylaminopropylsiloxy ligand on the central silicon (5). Pc 4-PDT generates ROS primarily within mitochondria, which leads to mitochondria-mediated apoptotic events that include the mitochondrial permeability transition, mitochondrial swelling and cytochrome *c* release (6). Other analogs of Pc 4 that primarily localize to lysosomes, however, are more effective in killing cancer cells than

* This work was supported, in whole or in part, by grants from the U. S. National Cancer Institute R01 CA119079 (A.-L. N.), P30 CA138313 (Hollings Cancer Center Cell and Molecular Imaging Shared Resource), Abney Cancer Foundation (H.-I. H.), and a scholarship from the government of Taiwan (H.-I. H.).

[1] To whom correspondence should be addressed: Dept. of Drug Discovery and Biomedical Sciences, Medical University of South Carolina, DD505 Drug Discovery Bldg., 70 President St., Charleston, SC. Tel.: 843-876-2361; Fax: 843-876-2353; E-mail: nieminen@musc.edu.

[2] The abbreviations used are: PDT, photodynamic therapy; DFO, desferrioxamine; MCU, mitochondrial calcium uniporter; Mfrn1, mitoferrin1; Mfrn2, mitoferrin-2; $OH^{\bullet}$, hydroxyl radical; PI, propidium iodide; ROS, reactive oxygen species; Ru360, ruthenium 360; sDFO, starch-desferrioxamine; TMRM, tetramethylrhodamine methyl ester.

the parent compound Pc 4, which localizes predominantly to mitochondria (7). Enhanced PDT efficacy is partly due to a release of lysosomal constituents such as cathepsins to the cytosol (8, 9).

Cellular iron exists in two pools: non-chelatable iron that is bound to ferritin and prosthetic groups (heme, iron-sulfur complexes, etc.) of proteins and chelatable iron that is either free or relatively loosely bound to anionic metabolites such as citrate and ATP. Chelatable but not non-chelatable iron is accessible for complex formation with chelators such as desferrioxamine (DFO). Lysosomes store substantial amounts of chelatable iron, which when released enhances PDT efficacy (10, 11). Chelatable iron promotes oxidative stress by catalyzing the Fenton reaction, which produces highly reactive hydroxyl radical ($OH^{\bullet}$) from H_2O_2 and $O_2^{\bullet-}$ (12). $OH^{\bullet}$ damages DNA, proteins, and membranes.

Under physiological conditions, cytosolic chelatable iron concentration is low. However, in pathological conditions, chelatable iron released from lysosomes can dramatically increase cytosolic iron concentration (11, 13). Mitochondria rapidly accumulate chelatable iron released by lysosomes via the electrogenic mitochondrial calcium uniporter (MCU) (11, 14–16). MCU has recently been characterized as a 40-kDa mitochondrial membrane protein with channel activity (15, 16). In addition to Ca^{2+}, MCU also transports Fe^{2+} into mitochondria when cytosolic Fe^{2+} is elevated (11, 14).

Another mitochondrial protein, mitoferrin (Mfrn), also has been reported to mediate iron transport across the mitochondrial inner membrane (17–19). Mfrn has two isoforms. Mfrn1 (SLC25A37) is a 38-kDa protein that is highly expressed in erythroid cells and in low levels in other tissues, whereas Mfrn2 (SLC25A28), a 39-kDa protein, is expressed in non-erythroid tissues (20–23). The relative extent to which MCU and Mfrn contribute to mitochondrial iron uptake and how these proteins interact is poorly understood.

In this study, we explored the potential contribution of Mfrn2 to PDT-mediated mitochondrial dysfunction and cytotoxicity after release of lysosomal iron with bafilomycin. Our findings indicate that lysosomal iron release and mitochondrial iron uptake through Mfrn2 act synergistically to induce PDT-mediated and iron-dependent mitochondrial dysfunction and subsequent cell killing. To our knowledge, this is the first study to show the causal link between Mfrn2 and mitochondrial dysfunction under pathological conditions.

EXPERIMENTAL PROCEDURES

Cell Culture—Human head and neck squamous carcinoma cell lines (UMSCC1, UMSCC14, and UMSCC22) were a gift from Dr. Besim Ogretmen (Medical University of South Carolina). Cells were cultured on 10-cm (3×10^6/dish), 6-cm (360,000/dish), 35-mm glass-bottomed MatTek dishes (MatTek Corp.; 150,000/dish), 24-well plates (100,000 and 200,000/well for UMSCC1 and UMSCC22A, respectively), and 96-well plates (6,000 and 15,000/well for UMSCC1 and UMSCC22A, respectively) in Dulbecco's modified Eagle's medium (DMEM) (Invitrogen) supplemented with 10% fetal bovine serum (FBS) and penicillin/streptomycin (complete culture medium) in a humidified 37 °C incubator at 5% CO_2, 95% air.

Cellular Pc 4 Uptake—The phthalocyanine photosensitizer Pc 4 was obtained from Dr. Malcolm Kenney (Case Western Reserve University) (5). A stock solution of 0.5 mM was prepared in dimethyl formamide and diluted into complete culture medium. At 24 h after replating, cells were incubated with Pc 4 at indicated concentrations for 18 h and then washed twice with PBS and lysed in 0.5% SDS. Cell lysates were collected, and fluorescence was measured with a fluorometer (Photon Technology International, Birmingham, NJ) using 610-nm excitation and 630–720-nm emission. A calibration curve was constructed by adding known concentrations of Pc 4 to the lysates.

Laser Scanning Confocal Microscopy—Glass-bottomed MatTek dishes were placed in an environmental chamber at 37 °C on the stage of a Zeiss LSM 510 laser scanning confocal microscope (Zeiss, Thornwood, NY). A 63 × numerical aperture 1.4 oil immersion planapochromat objective was used for all experiments. Rhodamine 123 and Pc 4 fluorescence was imaged using 488-nm excitation/500–530-nm emission and 543-nm excitation/560-nm long pass emission, respectively. Tetramethylrhodamine methylester (TMRM) fluorescence was imaged using 543-nm excitation and 560-nm long pass emission. Cells in images were outlined using Adobe Photoshop software (Mountain View, CA). Average TMRM fluorescence intensity of the outlined cells was then quantified followed by background subtraction to yield cell specific mean TMRM fluorescence intensity.

Subcellular Localization of Pc 4—UMSCC1, UMSCC14A, and UMACC22A cells were cultured onto glass-bottomed MakTek dishes and loaded with Pc 4 for 18 h. Medium was changed to fresh medium supplemented with insulin-transferrin-selenium-X reagent (insulin (10 μg/ml), transferrin (5.5 μg/ml), selenium (6.7 ng/ml), ethanolamine (0.2 mg/ml)) (Invitrogen) but omitting FBS. To assess co-localization of Pc 4 with mitochondria, cells were loaded with 500 nM rhodamine 123 for 20 min. Medium was then changed with fresh medium containing 50 nM rhodamine 123. Images of rhodamine 123 and Pc 4 were collected with confocal microscopy.

Photodynamic Therapy—Cell cultures were incubated with different concentrations of Pc 4 for 18 h before exposure to 390 mJ/cm^2 red light (670 nm) at 37 °C from an Intense HPD 7404 diode laser (North Brunswick, NJ). After exposure to red light, cells were incubated for various periods of time prior to analysis.

Mitochondrial Iron Uptake—UMSCC1 and UMSCC22A cells were cultured on 24-well plates for 24 h. Cells were then washed three times with intracellular buffer as follows (120 mM KCl, 10 mM NaCl, 2 mM $MgCl_2$, 2.5 mM KH_2PO_4, 20 mM HEPES buffer, pH 7.4, 0.02 mM EGTA, 5 mM Na_2 succinate, 2 mM ATP, 3 mM glutathione, 1 μM rotenone, 2 μM thapsigargin, 5 μM oligomycin, and 1 μg/ml protease inhibitors pepstatin, antipain, and leupeptin). Digitonin (10 μM) was added to the last wash. After 10 min, buffer was substituted with intracellular buffer containing 5 μM calcein-free acid (Molecular Probes), but no EGTA or digitonin and incubated for 5 min. Calcein does not enter mitochondria and thus localizes exclusively to the extracellular space. Calcein fluorescence (495-nm excitation/515-nm emission) was measured using a fluorescence

plate reader (Novostar, BMG LabTechnologies, Offenburg, Germany) at 37 °C. After collection of base-line fluorescence, 5 μM $FeSO_4$ was added, and fluorescence was measured every 0.5 s for 120 s. Fe^{2+} binds to calcein in 1:1 ratio resulting in quenching of calcein fluorescence (11, 24–26). As mitochondria take up Fe^{2+}, extramitochondrial calcein fluorescence becomes unquenched. Rates of decrease of fluorescence were normalized to protein content, and Fe^{2+} uptake was expressed as μmol Fe^{2+}/min/mg protein.

Mitochondrial Membrane Potential—Cells incubated with Pc 4 as described above were loaded with 250 nM TMRM for 60 min in culture medium followed by 50 nM TMRM to maintain equilibrium distribution of the fluorophores. After collecting base-line images of red TMRM fluorescence, cells were exposed to light (390 mJ/cm^2), and images were subsequently collected over time using confocal microscopy.

Assessment of Cell Death—Cell death was assessed by propidium iodide (PI) fluorometry using a multiwell fluorescence plate reader as described previously (27). PI fluorescence was measured at frequent intervals using 530-nm excitation (25-nm band pass) and 620-nm emission (40-nm band pass) filters. Between measurements, microtiter plates were placed in a 37 °C incubator. At the end of the experiment, digitonin (200 μM) was added to each well to permeabilize all cells and label all nuclei with PI. Cell viability determined by PI fluorometry is essentially the same as cell viability determined by trypan blue exclusion (27).

RNAi Knockdown—UMSCC22A cells in 10-cm Petri dishes were transfected with human Mfrn2 (Ambion Silencer Select, catalog no. 4392420, Gene SLC25A28-S37874) and non-target siRNA (25 nM, Ambion) using Lipofectamine RNAiMAX transfection reagent (Invitrogen) by reverse transfection according to the manufacturer's instructions. After 3 days, cells were trypsinized and plated on 24-well plates (50,000 cells) for a second siRNA transfection. After 3 more days, cells were loaded with Pc 4 for PDT experiments, as described above.

Quantitative Real Time PCR—Total mRNA was extracted from cell lysates using an RNeasy Mini Kit (Qiagen) following the manufacturer's instructions. Quantitative real time PCR was performed by a two-step procedure. cDNA was synthesized by an iScript cDNA Synthesis kit (Bio-Rad), and PCR was carried out using iQSYBR Green Supermix (Bio-Rad). Relative Mfrn gene expression was normalized to r18S as a gene expression control. Primers for Mfrn1 and Mfrn2 were adopted from Harvard Gene Bank as follows: Mfrn1 (ID 7706150a1)-fw, 5′-TAGCCAACGGGATAGCTGG-3′ and Mfrn1-rv, 5′-GTGGTGTAGCTCCGGTAGAAG-3′ (178 base pairs); Mfrn2 (ID 28703800a1)-fw, 5′-CTGCGTGATGTACCCCATCG-3′ and Mfrn2-rv, 5′-CCTGTTGCTGTGACGTTCAG-3′ (159 base pairs); 18S-fw, 5′-GAGGGAGCCTGAGAAACGG-3′; and 18S-rv, 5′-GTCGGGAGTGGGTAATTTGC-3′ (68 base pairs).

Western Blot Analysis—Cell extracts were prepared in ice-cold radioimmune precipitation assay lysis buffer (150 mM NaCl, 1 mM EGTA, 1% sodium deoxycholate, 1% Triton X-100, 0.1% SDS, 1% Nonidet P-40, 50 mM Tris-Cl, pH 7.4) supplemented with a mixture of protease inhibitors (Roche Diagnostics) and centrifuged. Equivalent amounts of protein determined by Bradford assay (Bio-Rad) in sample buffer (Invitrogen) supplemented with 10% SDS and 10% β-mercaptoethanol were resolved on NuPAGE® Tris-bis 4–12% polyacrylamide gels (Invitrogen). Proteins were transferred to PVDF membranes (EMD Millipore) and probed with anti-Mfrn-2 (1:500) (Abcam), anti-TOM20 (1:1000) (Santa Cruz Biotechnology), and anti-β-tubulin (1:1000) (Sigma-Aldrich). Membranes were developed by the Enhanced Chemiluminescence Detection System (Thermo Fisher Scientific), and band intensities were quantified using a Caresteam 4000 PRO image station (Woodbridge, CT).

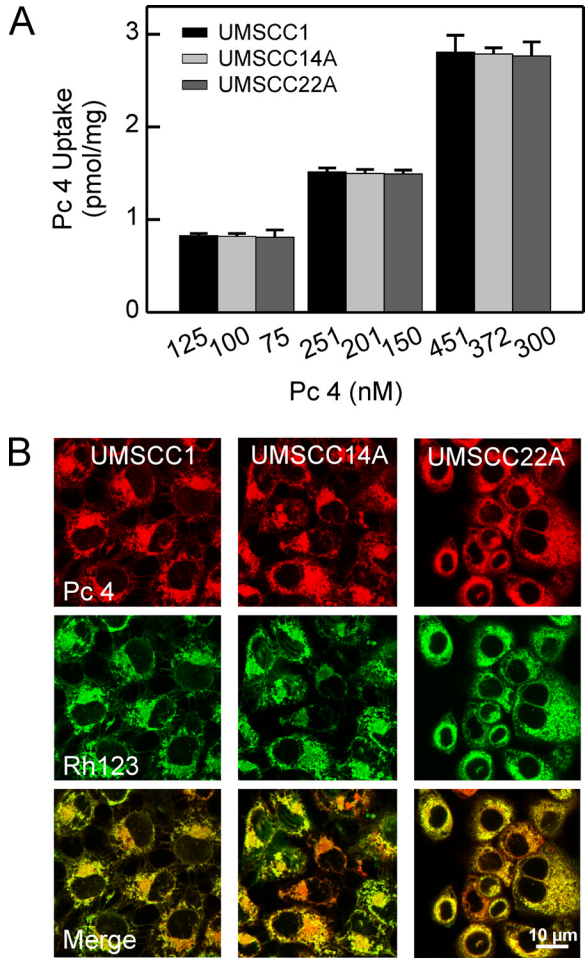

FIGURE 1. **Cellular uptake and subcellular localization of Pc 4 in head and neck cancer cells.** In *A*, UMSCC22A, UMSCC14A, and UMSCC1 cells were incubated with 75–300, 100–372, and 125–451 nM Pc 4, respectively, for 18 h in complete culture medium. Cells were lysed, and Pc 4 was measured spectrofluorometrically, as described under "Experimental Procedures." Values were normalized to protein and represent three independent experiments. In *B*, UMSCC1, UMSCC14A, and UMSCC22A cells were incubated with 251, 201, and 150 nM Pc 4, respectively, for 18 h. These loading concentrations achieved virtually equal Pc 4 uptake (1.5 pmol/mg protein) in three cell lines, as shown in *A*. Subsequently, cells were loaded with rhodamine 123 (*Rh123*), and green rhodamine 123 and far red Pc 4 fluorescence was imaged by confocal microscopy, as described under "Experimental Procedures." Images are representative of three independent experiments.

Statistical Analysis—Data are shown as means ± S.E. from at least three independent experiments performed in triplicate. Pairwise comparison was performed by two-tailed t test using Instat2 software (GraphPAD, San Diego, CA). A p value < 0.05 was considered to be statistically significant.

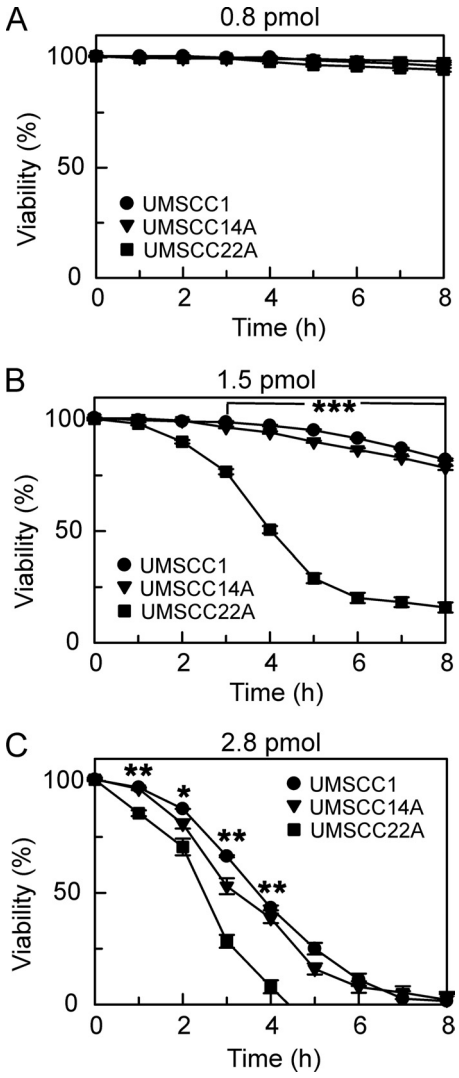

FIGURE 2. **Head and neck cancer cells respond differently to PDT.** Cells on 96-well plates were incubated for 18 h with Pc 4 to yield cellular Pc 4 loading 0.8, 1.5, and 2.8 pmol/mg protein (*A*, *B*, and *C*, respectively), as described in Fig. 1*A*. Cells were then placed in fresh medium supplemented with insulin-transferrin-selenium-X reagent and PI (30 μM) but omitting FBS followed by exposure to light, as described under "Experimental Procedures." Viability was assessed by PI fluorometry. Data represent three independent experiments performed in quadruplicate. *, $p < 0.05$; **, $p < 0.01$; ***, $p < 0.0001$ compared UMSCC1 and UMSCC14A to UMSCC22A.

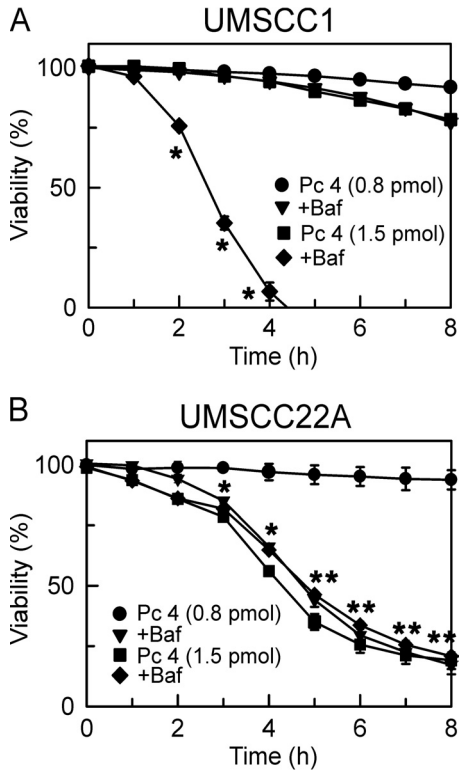

FIGURE 3. **Bafilomycin enhances PDT killing in resistant and sensitive cell lines.** UMSCC1 (*A*) and UMSCC22A (*B*) cells plated on 96-well plates were incubated with Pc 4 to yield loading of 0.8 and 1.5 pmol/mg protein, as described in Fig. 1*A*. After 18 h, medium was changed to fresh medium supplemented with insulin-transferrin-selenium-X reagent and PI (30 μM) but omitting FBS, followed by incubation with bafilomycin (*Baf*, 50 nM) for 1 h, where indicated. Subsequently, cells were exposed to light. Viability was assessed by PI fluorometry. Data represent three independent experiments performed in quadruplicate. *, $p < 0.0001$ compared with Pc 4 (1.5 pmol) (*A*). *, $p < 0.01$; **, $p < 0.001$ compared with Pc 4 (0.8 pmol) (*B*).

RESULTS

Cellular Uptake and Subcellular Localization of Pc 4 in Head and Neck Cancer Cells—Pc 4 is a hydrophobic photosensitizer that diffuses freely across the plasma membrane and binds to membranes of intracellular organelles (6). Based on preliminary experiments, the three head and neck cancer cell lines were incubated with different concentrations of Pc 4, as indicated in Fig. 1*A*. Cellular Pc 4 uptake was determined in cell lysates. The three cell lines took up Pc 4 differently in the order of UMSCC22A > UMSCC14A > UMSCC1 (Fig. 1*A*). UMSCC14A and UMSCC1 cells required higher loading concentrations of Pc 4 to yield the same Pc 4 uptake as UMSCC22A cells (Fig. 1*A*). Subsequent studies utilized Pc 4 loading concentrations described in Fig. 1*A* to achieve nearly equal Pc 4 loading of 0.8, 1.5 and 2.8 pmol/mg protein for the three cell types. Subcellular localization of Pc 4 was determined at equal cellular Pc 4 loading (1.5 pmol/mg) using confocal microscopy. To determine co-localization of Pc 4 with mitochondria, cells were loaded with rhodamine 123, a green-fluorescing mitochondria-specific probe. Most far red-fluorescing Pc 4 co-localized with rhodamine 123-labeled mitochondria, as shown by yellow in the merged green and red fluorescence images (Fig. 1*B*). In all three cell lines, the overall Pc 4 pattern and co-localization of Pc 4 with rhodamine 123 were similar (Fig. 1*B*).

Head and Neck Cancer Cells Respond Differently to PDT—After determination of Pc 4 loading concentrations resulting in equal cellular Pc 4 uptake between the three head and neck cancer cell lines, we determined their individual sensitivity to Pc 4-PDT. Sensitivity to Pc 4-PDT was determined at three different levels of cellular Pc 4 uptake: 0.8, 1.5, and 2.8 pmol/mg protein. All three cell lines were resistant to PDT at Pc 4 uptake of 0.8 pmol/mg protein (Fig. 2*A*). At 1.5 pmol/mg protein, Pc 4-PDT had minimal toxicity in UMSCC1 and UMSCC14A cells, but UMSCC22A cells were more sensitive. In UMSCC22A cells, viability decreased to 15% at 8 h after PDT with 1.5 pmol of Pc 4/mg protein (Fig. 2, *A* and *B*). At still higher Pc 4 (2.8 pmol/mg), the differences in sensitivity between cell lines diminished, although UMSCC22A cells still showed the fastest rate of cell killing (Fig. 2*C*). Because resistant UMSCC1 and UMSCC14A cells were similar in sensitivity to PDT, we

focused on UMSCC1 cells in comparison with UMSCC22A cells for further experiments.

Bafilomycin Enhances PDT Killing in Both Resistant and Sensitive Cell Lines—Our previous studies showed that collapse of lysosomal pH by bafilomycin, an inhibitor of the vacuolar proton-pumping ATPase (V-ATPase), enhances mitochondria-mediated Pc 4-PDT killing in A431 epidermoid cancer cells (10). Here, we assessed the effect of bafilomycin on PDT-induced cell killing in head and neck cancer cell lines. At a loading of 0.8 pmol/mg protein, Pc 4-PDT alone or in combination with bafilomycin induced minimal toxicity in resistant UMSCC1 cells (Fig. 3*A*). At higher Pc 4 loading (1.5 pmol/mg), the combination of Pc 4 with bafilomycin caused 100% cell death within 5 h after PDT (Fig. 3*A*). In these experiments, bafilomycin alone and light alone caused no toxicity (data not shown).

In sensitive UMSCC22A cells, Pc 4 at 0.8 pmol/mg protein caused no toxicity during PDT, but the combination of Pc 4 with bafilomycin greatly enhanced cell killing and decreased viability from 93% (Pc 4-PDT alone) to 17% (Pc 4-PDT plus bafilomycin) (Fig. 3*B*). At higher Pc 4 (1.5 pmol/mg), PDT induced substantial cell killing in sensitive UMSCC22A cells, and bafilomycin did not further enhance killing since the UMSCC22 cells were already very sensitive to the higher Pc 4 dose. We obtained similar results with another agent, chloroquine, which, similar to bafilomycin, causes lysosomal alkalinization (data not shown) (28, 29). Bafilomycin and chloroquine induce lysosomal alkalinization by different mechanisms: bafilomycin inhibits V-ATPase, whereas chloroquine is a weak base that accumulates into lysosomes to collapse the acidic pH gradient. Acidic lysosomal digestion of iron-containing proteins is one source of intralysosomal chelatable iron. However, the lysosomal protease inhibitors pepstatin A and leupeptin (10 μM) did not alter PDT-induced cell death in either the presence or absence of bafilomycin (data not shown). Taken together, the results in Figs. 2 and 3 demonstrated that bafilomycin sensitizes both sensitive and resistant head and neck cancer cell lines to Pc 4-PDT. Resistant cells are sensitized by bafilomycin and relatively higher Pc 4 loading, whereas sensitive cells were sensitized at lower Pc 4 loading.

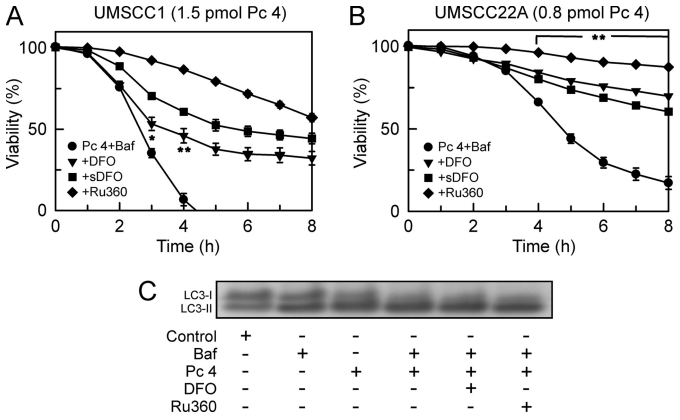

FIGURE 4. **Iron chelators and Ru360 protect against bafilomycin-enhanced PDT killing.** UMSCC1 (*A*) and UMSCC22A (*B*) cells were loaded with Pc 4 in the presence and absence of iron chelators, DFO (1 mM) and sDFO (1 mM), and the MCU inhibitor, Ru360 (10 μM) for 18 h. Cells were exposed to light, and cell killing was assessed with PI fluorometry, as described in Fig. 2. Values are from three independent experiments. *, $p < 0.05$; **, $p < 0.01$ compared Pc 4+bafilomycin+DFO/sDFO/Ru360 to Pc 4+bafilomycin (*Baf*). In *C*, UMSCC22A cell lysates collected at 45 min post-PDT were analyzed by Western blotting for LC3-I and II. Blot is representative of four independent experiments.

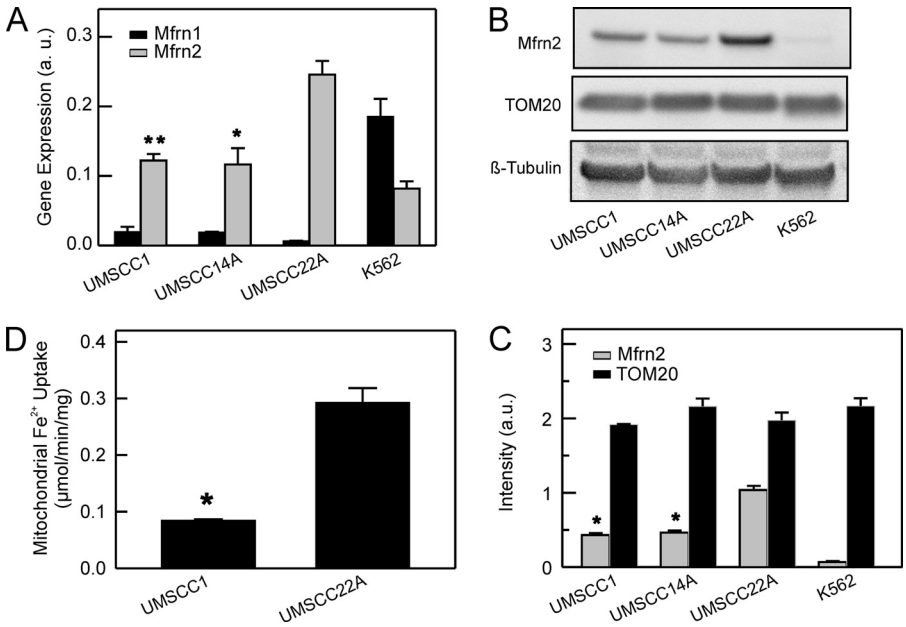

FIGURE 5. **Differential endogenous Mfrn2 gene and protein expression in head and neck cancer cells.** In *A*, Mfrn1 and Mfrn2 mRNA were quantified in different cell types by real time PCR, as described under "Experimental Procedures." Values are expressed as arbitrary units (*a. u.*) normalized to the housekeeping rRNA 18S. Data are from three independent lysates. *, $p < 0.05$; **, $p < 0.01$ compared with UMSCC22A. In *B* and *C*, cell lysates were analyzed by Western blotting for Mfrn2, TOM20, and β-tubulin. Blots are representative of three independent experiments (*B*). Band intensities were quantified and normalized to β-tubulin (*C*). Data are from three independent lysates. *, $p < 0.0001$ compared with UMSCC22A. In *D*, UMSCC1 and UMSCC22A cells were incubated in intracellular buffer, and rates of the mitochondrial Fe^{2+} uptake were measured after digitonin-permeabilization from dequenching of calcein fluorescence, as described under "Experimental Procedures." Data represent three independent experiments performed in triplicate. *, $p < 0.01$ compared with UMSCC22A.

Iron Chelators and Ru360 Protect Against Bafilomycin-enhanced PDT Killing—Bafilomycin releases chelatable iron from lysosomes to the cytosol (11). Therefore, we characterized whether chelation of iron would protect against bafilomycin-enhanced cell killing during PDT. Cells were pretreated with DFO (1 mM) for 18 h before bafilomycin and subsequent light exposure. In resistant UMSCC1 cells, DFO protected against cell killing and increased cell viability from 0 to 37% at 5 h after PDT with high Pc 4 (1.5 pmol/mg) (Fig. 4*A*). sDFO (1 mM, Biomedical Frontiers, St. Paul, MN), which is taken up by endocytosis and specifically chelates endosomal/lysosomal iron, protected against cell killing after Pc 4-PDT to an even greater extent than DFO, increasing viability from 0 to 52% after 5 h (Fig. 4*A*). Ru360 is a highly specific inhibitor of the electrogenic MCU (30). When cytosolic Fe^{2+} increases, MCU transports iron into mitochondria (11, 14). Ru360 (10 μM) blocked bafilomycin-enhanced PDT killing, increasing viability from 0 to 79% after 5 h in UMSCC1 cells (Fig. 4*A*).

Similarly, in sensitive MUSCC22A cells, DFO and sDFO greatly protected against bafilomycin-enhanced PDT toxicity at low Pc 4 (0.8 pmol/mg), increasing viability from 17% to 69 and 60%, respectively, after 8 h (Fig. 4*B*). Ru360 provided even greater protection and increased viability from 17 to 87%. Cytoprotection with sDFO indicated that bafilomycin-enhanced toxicity during PDT is mediated by release of lysosomal iron to the cytosol, whereas protection by Ru360 implies that mitochondrial iron uptake by MCU also underlies PDT.

Bafilomycin and chloroquine block processing of autophagosomes and prevent autophagy by accumulation of LC3-II (31–33). To exclude the possibility that DFO or Ru360 affect autophagy, LC3-II protein expression was determined in UMSCC22A cells. Bafilomycin plus Pc 4-PDT increased LC3-II protein expression (Fig. 4*C*). However, DFO and Ru360 did not have additional effect on LC3-II, indicating that cytoprotection by DFO and Ru360 cannot be explained by changes in autophagy.

Differential Endogenous Mfrn2 Gene and Protein Expression in Head and Neck Cancer Cells—In non-erythroid cells, Mfrn2 is an iron transporter localized in the mitochondrial inner membrane that transports iron from the cytosol into mitochondria (20, 34). Because bafilomycin-induced toxicity during PDT is likely related to mitochondrial iron uptake, we assessed Mfrn2 expression in head and neck cancer cells. PDT-sensitive cells (UMSCC22A) expressed 2-fold higher Mfrn2 mRNA measured by quantitative PCR compared with PDT-resistant (UMSCC1 and UMSCC14A) cells. As expected, all head and neck cancer cells expressed little Mfrn1, the isoform expressed predominantly in hematopoietic cells (Fig. 5*A*). Conversely, human 562 erythromyeloblastoid leukemia cells expressed high levels of Mfrn1 and less Mfrn2 (Fig. 5*A*).

As assessed by Western immunoblotting, PDT sensitive UMSCC22A expressed 2-fold higher Mfrn2 protein levels compared with resistant UMSCC1 and UMSCC14A (Fig. 5, *B* and *C*). Lys-562 cells expressed much lower Mfrn2 (Fig. 5, *B* and *C*). Samples from all cell lines contained equal amounts of the mitochondria-specific protein TOM20 (Fig. 5*C*). Thus, the difference in Mfrn2 protein expression between the cell lines cannot be explained by differences in mitochondrial proteins in lysates.

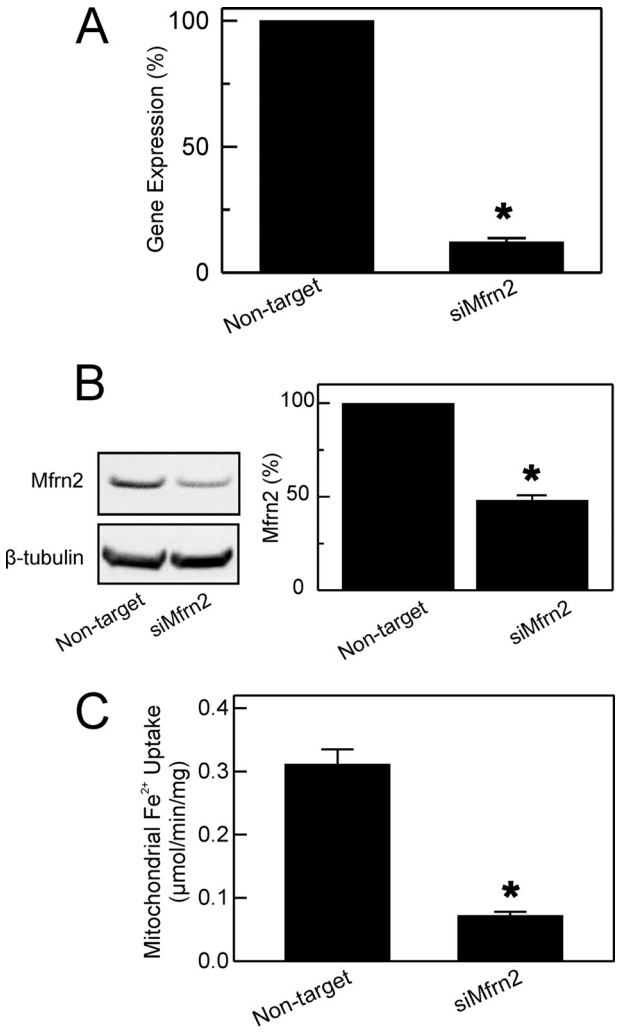

FIGURE 6. **Mfrn2 knockdown decreases mitochondrial iron uptake.** UMSCC22A cells were transfected with Mfrn2 and non-target siRNA for 6 days, as described in "Experimental Procedures." In *A*, Mfrn2 mRNA expression by real time PCR was normalized to 18S rRNA and expressed as percent of non-target values. Data are from three independent experiments. *, $p < 0.01$ compared with non-target siRNA. In *B*, protein expression of Mfrn2 and β-tubulin after siRNA treatments was quantified. A representative Western blot and averaged intensities from three independent experiments are shown. *, $p < 0.05$ compared with non-target siRNA. In *C*, mitochondrial Fe^{2+} uptake was measured in digitonin-permeabilized cells, as described under "Experimental Procedures." Data are from three independent experiments performed in triplicate. *, $p < 0.01$ compared with non-target siRNA.

Down-regulation of Mfrn2 Results in Decreased Mitochondrial Fe^{2+} Uptake—Next, we determined whether cells expressing more Mfrn2 were capable of transporting iron faster from the cytosol to mitochondria compared with cells with less Mfrn2. Mitochondrial iron uptake was measured in digitonin-permeabilized cells after addition of 5 μM $FeSO_4$ using calcein fluorescence, which is quenched by Fe^{2+}. Bafilomycin was not included in these experiments because any iron released by lysosomes would have been immediately diluted into the medium. Indeed, PDT-sensitive UMSCC22A cells showed higher rates of mitochondrial Fe^{2+} uptake compared with resistant UMSCC1 cells (0.27 *versus* 0.08 μmol Fe^{2+}/min/mg

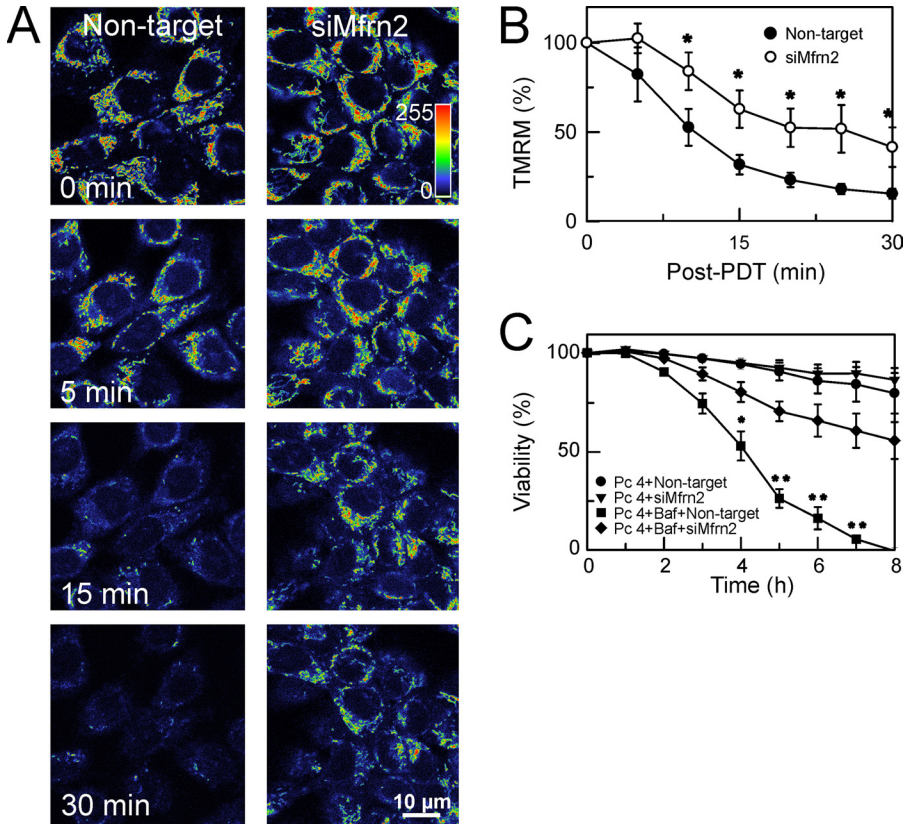

FIGURE 7. **Mfrn2 knockdown confers resistance to mitochondrial depolarization and cell killing after PDT.** In *A*, UMSCC22A cells were transfected with Mfrn2 and non-target siRNA for 6 days, as described under "Experimental Procedures." Cells were then incubated with Pc 4 (0.8 pmol/mg protein) for 18 h in complete culture medium, loaded with TMRM, as described under "Experimental Procedures." Red fluorescence of TMRM was imaged by laser scanning confocal microscopy before (0 min) and every 5 min after irradiation for 30 min. Image intensity was pseudocolored according to the reference bar. Representative images from three independent experiments are shown. In *B*, average TMRM fluorescence after background subtraction under conditions described in *A* is plotted as percentage of TMRM fluorescence of 0 min. Data are from analysis of 74–80 cells per treatment group obtained from three independent experiments. *, $p < 0.05$ compared with non-target siRNA. In *C*, cells viability under the same conditions as *A* was determined by PI fluorometry. Data represent three independent experiments performed in quadruplicate. *, $p < 0.05$ compared with non-target siRNA. *Baf*, bafilomycin.

protein) (Fig. 5*C*). Ru360 (10 μM) blocked Fe^{2+} uptake virtually completely in both cell lines (data not shown).

The results in Fig. 5 demonstrate a correlation between Mfrn2 expression and mitochondrial Fe^{2+} uptake in head and neck cancer cells. Therefore, we reasoned that decreased expression of Mfrn2 in UMSCC22A cells should also decrease mitochondrial Fe^{2+} uptake. Knockdown of Mfrn2 in UMSCC22A cells using siRNA caused an 88% decrease in Mfrn2 gene expression (Fig. 6*A*) and a 56% decrease in protein expression (Fig. 6*B*). As expected, knockdown of Mfrn2 also decreased rates of mitochondrial Fe^{2+} uptake by 79% compared with cells transfected with non-target siRNA (0.31 *versus* 0.07 μmol/min/mg protein) (Fig. 6*C*).

Down-regulation of Mfrn2 Delays Mitochondrial Depolarization and Cell Death after PDT Plus Bafilomycin—Iron, by participating in Fenton chemistry and increasing ROS production, can induce mitochondrial dysfunction and cell death. Therefore, we assessed the effects of Mfrn2 knockdown on mitochondrial membrane potential and cell viability in high Mfrn2-expressing UMSCC22A cells. At 0 min, bright pseudocolored red and yellow spheres represented high TMRM fluorescence intensities in polarized mitochondria (Fig. 7*A*). After exposure to PDT with low Pc 4 (0.8 pmol/mg protein) plus bafilomycin, bright spheres rapidly disappeared in cells transfected with non-target siRNA, such that after 15 min, most TMRM had leaked from the mitochondria, indicating mitochondrial depolarization. After 30 min, virtually all polarized mitochondria disappeared (Fig. 7, *A* and *B*). By contrast in Mfrn2 knockdown cells, many brightly fluorescent mitochondria persisted even after 30 min (Fig. 7*A*). These differences were statistically significant (Fig. 7*B*). Moreover, Mfrn2 knockdown protected against cell killing after PDT with bafilomycin, increasing cell viability from 0 to 56% after 8 h (Fig. 7*C*). The results implicate Mfrn2 expression as a key factor in sensitivity to Pc 4-PDT.

DISCUSSION

This study provides mechanistic information regarding the contribution of lysosomal chelatable iron to mitochondrial dysfunction and cell death during PDT. Our results indicate that lysosomal iron release and mitochondrial iron uptake through Mfrn2 act synergistically to induce PDT-mediated and iron-dependent mitochondrial dysfunction and subsequent cell killing in head and neck cancer cells. To our knowledge, this is the first study to show that Mfrn2 participates in mitochondrial dysfunction under pathological conditions.

Treatment of head and neck cancers is especially challenging because current treatments such as surgery drastically affect patient quality of life. PDT has been successfully used for head

and neck squamous carcinomas in a number of clinical trials using different photosensitizers (35, 36). In this study of different head and neck cancer cell lines exposed to Pc 4-PDT, UMSCC1 and UMSCC14A were more resistant than UMSCC22A to Pc 4-PDT (Fig. 2). Differences in sensitivity could not be explained by differences in uptake or sub-cellular localization of Pc 4 (Fig. 1).

During Pc 4-PDT, the predominant proportion of ROS production occurs inside mitochondria, leading to the mitochondrial permeability transition and cell death (6). Our previous results showed that lysosomal iron release by bafilomycin greatly accelerates Pc 4-PDT-mediated cell killing in A431 epidermoid carcinoma cells (10). Although bafilomycin acts on lysosomes, its toxic effects are manifested in mitochondria by accelerated depolarization after PDT, resulting in cell death (10). Lysosomes are a reservoir of chelatable, redox-active Fe^{2+} (11). Fe^{2+} reacts with H_2O_2 to generate highly reactive and toxic $OH^{\bullet}$. Once released from lysosomes by bafilomycin, iron can participate in iron-mediated Fenton chemistry in the cytosol or be taken up by mitochondria to catalyze mitochondrial ROS production. Bafilomycin enhanced PDT cell killing in all three head and neck cancer cell lines studied, although there was a difference in sensitivity to bafilomycin among the cell lines (Fig. 3). Chloroquine, another lysosomal alkalinizing agent, also promoted PDT toxicity (data not shown).

UMSCC22A cells that were most sensitive to PDT alone were also most sensitive to bafilomycin-enhanced toxicity during PDT (Fig. 3). The iron chelators DFO and sDFO both protected against bafilomycin-enhanced PDT toxicity (Fig. 4). The observation that sDFO, which specifically chelates lysosomal iron, was also cytoprotective indicates that lysosomes/endosomes release redox-active chelatable iron after bafilomycin and that DFO and sDFO prevent this release by chelating the intraluminal iron store of these organelles. As shown by increased LC3-II protein expression, bafilomycin plus Pc 4-PDT enhanced accumulation of autophagosomes. However, DFO and Ru360 did not change LC3-II protein expression, signifying that cytoprotection by DFO and Ru360 was not mediated by changes of autophagy (Fig. 4*C*).

Ru360 also protected against bafilomycin-enhaced PDT toxicity (Fig. 4). Interestingly, Ru360-mediated protection was greater than that observed with iron chelators. Ru360 is a potent inhibitor of the MCU (30). For years, Ca^{2+} uptake across the mitochondrial inner membrane has been known to be mediated by MCU. However, only recently, MCU was identified as a 40-kDa mitochondrial inner membrane protein. MCU contains two transmembrane domains and shows channel activity (15, 16). MCU also mediates transport of Fe^{2+} into mitochondria, and DFO- and sDFO-sensitive mitochondrial iron uptake through MCU occurs in pathological situations and contributes to cytotoxicity (11, 14, 29). Therefore, Ru360 protection against bafilomycin toxicity during PDT is likely explained by prevention of Fe^{2+} uptake into mitochondria through MCU.

Although MCU may serve as an iron transporter under pathological conditions, other iron transporters have been identified as well. Mfrn1 is highly expressed in erythroid cells, whereas nonerythroid tissues express Mfrn2 (20). There is no

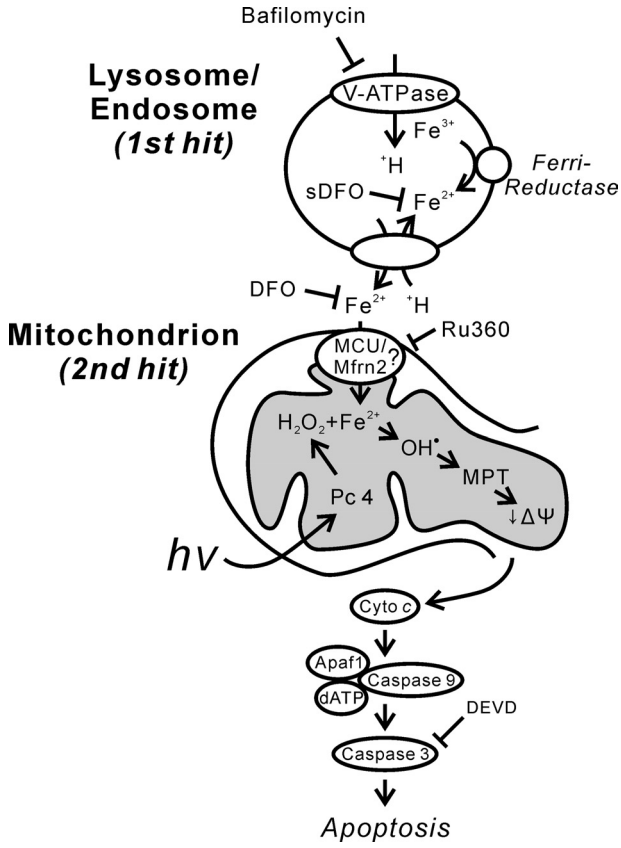

FIGURE 8. **Mfrn2 contributes to PDT-induced cell death.** Pc 4-PDT induces mitochondrial ROS production resulting in apoptotic cell death. The photosensitizer Pc 4 localizes to mitochondria and is activated by light (*hv*) to produce formation of intramitochondrial ROS, including H_2O_2. Iron released from lysosomes by bafilomycin is taken up by mitochondria in a Mfrn2-dependent fashion. Iron inside mitochondria participates in Fenton chemistry to further enhance the ROS-mediated mitochondrial permeability transition (MPT), mitochondrial depolarization, cytochrome *c* (*cyto c*) release and apoptotic cell death. Cytotoxicity is decreased by the iron chelators DFO and sDFO and by Ru360 that prevents mitochondrial iron uptake. Knockdown of Mfrn2 delays mitochondrial depolarization and cell death induced by bafilomycin during PDT.

sequence homology between MCU and Mfrn2 (15, 16). All three head and neck cancer cell lines expressed very little Mfrn1 (Fig. 5). Interestingly, the cell lines that were more resistant (UMSCC1 and UMSCC14A) to PDT and bafilomycin toxicity also expressed less Mfrn2 mRNA and protein than UMSCC22A, a sensitive cell line (Figs. 3 and 5). Furthermore, mitochondria in permeabilized UMSCC22A cells took up Fe^{2+} at a 3.6-fold faster rate compared with UMSCC1 cells (Fig. 5*C*). These findings suggest that Mfrn2 may be a regulator of MCU. The interaction between MCU and Mfrn2 is still unresolved. Immunoprecipitation does not show an interaction between MCU and Mfrn2 (16). However, this interaction may require higher Fe^{2+} compared with physiological conditions. Another possibility is that MCU and Mfrn2 are two entirely separate transporters, but both are inhibited by Ru360. Further studies are needed to address these questions.

Down-regulation of Mfrn2 decreased the rate of mitochondrial Fe^{2+} uptake and delayed mitochondrial depolarization and subsequent cell death after PDT plus bafilomycin (Figs. 6 and 7). These findings are consistent with the conclusion that Mfrn2-dependent mitochondrial Fe^{2+} uptake contributes to

cytotoxicity during PDT. The finding that Ru360 protected against bafilomycin-enhanced PDT toxicity also suggests that MCU-mediated mitochondrial Ca^{2+} uptake may contribute to PDT cytotoxicity, which would explain greater protection by Ru360 than DFO or sDFO (Fig. 4).

Our data support the conclusion that lysosomal iron release and mitochondrial iron uptake act synergistically to induce PDT-mediated and iron-dependent mitochondrial dysfunction and subsequent cell killing (Fig. 8). Pc 4 localized to mitochondria is activated by light to produce intramitochondrial ROS. Iron released from lysosomes by bafilomycin is taken up by mitochondria in a Mfrn2-dependent fashion, where it participates in iron-mediated Fenton reaction and further enhances ROS-mediated mitochondrial permeability transition onset, mitochondrial depolarization, cytochrome *c* release, and apoptotic cell death (6). Intracellular iron chelation by DFO and lysosomal iron chelation by sDFO protect against mitochondrial depolarization and cell death (10). Knockdown of Mfrn2 decreases mitochondrial iron uptake and also delays mitochondrial depolarization and cell death after PDT. Mfrn2-dependent mitochondrial iron uptake may also involve MCU because Ru360, a specific inhibitor of MCU, blocks Mfrn2-dependent iron uptake and protects against PDT cytotoxicity. Mfrn2 represents a possible biomarker of sensitivity of head and neck cancers to cell killing after PDT. Furthermore, adjuvant bafilomycin or chloroquine might enhance tumor response to Pc 4-PDT, especially in high Mfrn2-expressing tumors, by promoting iron-dependent ROS production.

Acknowledgments—We thank Dr. M. Kenney (Case Western Reserve University) for Pc 4 and Dr. Y. Manevich (Medical University of South Carolina) for help on use of fluorometer in Pc 4 uptake studies.

REFERENCES

1. Duvvuri, U., and Myers, J. N. (2009) Cancer of the head and neck is the sixth most common cancer worldwide. *Curr. Probl. Surg.* **46,** 114–117
2. Bihan, H., Baudin, E., Meas, T., Leboulleux, S., Al Ghuzlan, A., Hannoteaux, V., Travagli, J. P., Valleur, P., Guillausseau, P. J., and Cohen, R., and French Group of Endocrine Tumors (2012) Role of prophylactic thyroidectomy in RET 790 familial medullary thyroid carcinoma. *Head Neck* **34,** 493–498
3. Agostinis, P., Berg, K., Cengel, K. A., Foster, T. H., Girotti, A. W., Gollnick, S. O., Hahn, S. M., Hamblin, M. R., Juzeniene, A., Kessel, D., Korbelik, M., Moan, J., Mroz, P., Nowis, D., Piette, J., Wilson, B. C., and Golab, J. (2011) Photodynamic therapy of cancer: an update. *CA Cancer J. Clin.* **61,** 250–281
4. Baron, E. D., Malbasa, C. L., Santo-Domingo, D., Fu, P., Miller, J. D., Hanneman, K. K., Hsia, A. H., Oleinick, N. L., Colussi, V. C., and Cooper, K. D. (2010) Silicon phthalocyanine (Pc 4) photodynamic therapy is a safe modality for cutaneous neoplasms: results of a phase 1 clinical trial. *Lasers Surg. Med.* **42,** 728–735
5. Oleinick, N. L., Antunez, A. R., Clay, M. E., Rihter, B. D., and Kenney, M. E. (1993) New phthalocyanine photosensitizers for photodynamic therapy. *Photochem. Photobiol.* **57,** 242–247
6. Lam, M., Oleinick, N. L., and Nieminen, A. L. (2001) Photodynamic therapy-induced apoptosis in epidermoid carcinoma cells. Reactive oxygen species and mitochondrial inner membrane permeabilization. *J. Biol. Chem.* **276,** 47379–47386
7. Rodriguez, M. E., Zhang, P., Azizuddin, K., Delos Santos, G. B., Chiu, S. M., Xue, L. Y., Berlin, J. C., Peng, X., Wu, H., Lam, M., Nieminen, A. L., Kenney, M. E., and Oleinick, N. L. (2009) Structural factors and mechanisms underlying the improved photodynamic cell killing with silicon phthalocyanine photosensitizers directed to lysosomes versus mitochondria. *Photochem. Photobiol.* **85,** 1189–1200
8. Chiu, S. M., Xue, L. Y., Lam, M., Rodriguez, M. E., Zhang, P., Kenney, M. E., Nieminen, A. L., and Oleinick, N. L. (2010) A requirement for bid for induction of apoptosis by photodynamic therapy with a lysosome- but not a mitochondrion-targeted photosensitizer. *Photochem. Photobiol.* **86,** 1161–1173
9. Liu, L., Zhang, Z., and Xing, D. (2011) Cell death via mitochondrial apoptotic pathway due to activation of Bax by lysosomal photodamage. *Free Radic. Biol. Med.* **51,** 53–68
10. Saggu, S., Hung, H. I., Quiogue, G., Lemasters, J. J., and Nieminen, A. L. (2012) Lysosomal signaling enhances mitochondria-mediated photodynamic therapy in A431 cancer cells: role of iron. *Photochem. Photobiol.* **88,** 461–468
11. Uchiyama, A., Kim, J. S., Kon, K., Jaeschke, H., Ikejima, K., Watanabe, S., and Lemasters, J. J. (2008) Translocation of iron from lysosomes into mitochondria is a key event during oxidative stress-induced hepatocellular injury. *Hepatology* **48,** 1644–1654
12. Kehrer, J. P. (2000) The Haber-Weiss reaction and mechanisms of toxicity. *Toxicology* **149,** 43–50
13. Kurz, T., Gustafsson, B., and Brunk, U. T. (2011) Cell sensitivity to oxidative stress is influenced by ferritin autophagy. *Free Radic. Biol. Med.* **50,** 1647–1658
14. Flatmark, T., and Romslo, I. (1975) Energy-dependent accumulation of iron by isolated rat liver mitochondria. Requirement of reducing equivalents and evidence for a unidirectional flux of Fe(II) across the inner membrane. *J. Biol. Chem.* **250,** 6433–6438
15. De Stefani, D., Raffaello, A., Teardo, E., Szabò, I., and Rizzuto, R. (2011) A forty-kilodalton protein of the inner membrane is the mitochondrial calcium uniporter. *Nature* **476,** 336–340
16. Baughman, J. M., Perocchi, F., Girgis, H. S., Plovanich, M., Belcher-Timme, C. A., Sancak, Y., Bao, X. R., Strittmatter, L., Goldberger, O., Bogorad, R. L., Koteliansky, V., and Mootha, V. K. (2011) Integrative genomics identifies MCU as an essential component of the mitochondrial calcium uniporter. *Nature* **476,** 341–345
17. Shaw, G. C., Cope, J. J., Li, L., Corson, K., Hersey, C., Ackermann, G. E., Gwynn, B., Lambert, A. J., Wingert, R. A., Traver, D., Trede, N. S., Barut, B. A., Zhou, Y., Minet, E., Donovan, A., Brownlie, A., Balzan, R., Weiss, M. J., Peters, L. L., Kaplan, J., Zon, L. I., and Paw, B. H. (2006) Mitoferrin is essential for erythroid iron assimilation. *Nature* **440,** 96–100
18. Satre, M., Mattei, S., Aubry, L., Gaudet, P., Pelosi, L., Brandolin, G., and Klein, G. (2007) Mitochondrial carrier family: repertoire and peculiarities of the cellular slime mould *Dictyostelium discoideum*. *Biochimie* **89,** 1058–1069
19. Froschauer, E. M., Schweyen, R. J., and Wiesenberger, G. (2009) The yeast mitochondrial carrier proteins Mrs3p/Mrs4p mediate iron transport across the inner mitochondrial membrane. *Biochim. Biophys. Acta* **1788,** 1044–1050
20. Paradkar, P. N., Zumbrennen, K. B., Paw, B. H., Ward, D. M., and Kaplan, J. (2009) Regulation of mitochondrial iron import through differential turnover of mitoferrin 1 and mitoferrin 2. *Mol. Cell. Biol.* **29,** 1007–1016
21. Amigo, J. D., Yu, M., Troadec, M. B., Gwynn, B., Cooney, J. D., Lambert, A. J., Chi, N. C., Weiss, M. J., Peters, L. L., Kaplan, J., Cantor, A. B., and Paw, B. H. (2011) Identification of distal cis-regulatory elements at mouse mitoferrin loci using zebrafish transgenesis. *Mol. Cell. Biol.* **31,** 1344–1356
22. Troadec, M. B., Warner, D., Wallace, J., Thomas, K., Spangrude, G. J., Phillips, J., Khalimonchuk, O., Paw, B. H., Ward, D. M., and Kaplan, J. (2011) Targeted deletion of the mouse Mitoferrin1 gene: from anemia to protoporphyria. *Blood* **117,** 5494–5502
23. Ren, Y., Yang, S., Tan, G., Ye, W., Liu, D., Qian, X., Ding, Z., Zhong, Y., Zhang, J., Jiang, D., Zhao, Y., and Lu, J. (2012) Reduction of mitoferrin results in abnormal development and extended lifespan in *Caenorhabditis elegans*. *PLoS One* **7,** e29666
24. Messner, D. J., Sivam, G., and Kowdley, K. V. (2009) Curcumin reduces the toxic effects of iron loading in rat liver epithelial cells. *Liver Int.* **29,** 63–72
25. Breuer, W., Epsztejn, S., Millgram, P., and Cabantchik, I. Z. (1995) Trans-

port of iron and other transition metals into cells as revealed by a fluorescent probe. *Am. J. Physiol.* **268,** C1354-C1361
26. Li, Z., Tanaka, H., Galiano, F., and Glass, J. (2011) Anticancer activity of the iron facilitator LS081. *J. Exp. Clin. Cancer Res.* **30,** 34
27. Nieminen, A. L., Gores, G. J., Bond, J. M., Imberti, R., Herman, B., and Lemasters, J. J. (1992) A novel cytotoxicity screening assay using a multiwell fluorescence scanner. *Toxicol. Appl. Pharmacol.* **115,** 147–155
28. Poole, B., and Ohkuma, S. (1981) Effect of weak bases on the intralysosomal pH in mouse peritoneal macrophages. *J. Cell Biol.* **90,** 665–669
29. Kon, K., Kim, J. S., Uchiyama, A., Jaeschke, H., and Lemasters, J. J. (2010) Lysosomal iron mobilization and induction of the mitochondrial permeability transition in acetaminophen-induced toxicity to mouse hepatocytes. *Toxicol. Sci.* **117,** 101–108
30. Ying, W. L., Emerson, J., Clarke, M. J., and Sanadi, D. R. (1991) Inhibition of mitochondrial calcium ion transport by an oxo-bridged dinuclear ruthenium ammine complex. *Biochemistry* **30,** 4949–4952
31. Yamamoto, A., Tagawa, Y., Yoshimori, T., Moriyama, Y., Masaki, R., and Tashiro, Y. (1998) Bafilomycin A1 prevents maturation of autophagic vacuoles by inhibiting fusion between autophagosomes and lysosomes in rat hepatoma cell line, H-4-II-E cells. *Cell Struct. Funct.* **23,** 33–42
32. Kawai, A., Uchiyama, H., Takano, S., Nakamura, N., and Ohkuma, S. (2007) Autophagosome-lysosome fusion depends on the pH in acidic compartments in CHO cells. *Autophagy.* **3,** 154–157
33. Berg, T. O., Fengsrud, M., Strømhaug, P. E., Berg, T., and Seglen, P. O. (1998) Isolation and characterization of rat liver amphisomes. Evidence for fusion of autophagosomes with both early and late endosomes. *J. Biol. Chem.* **273,** 21883–21892
34. Carroll, C. B., Zeissler, M. L., Chadborn, N., Gibson, K., Williams, G., Zajicek, J. P., Morrison, K. E., and Hanemann, C. O. (2011) Changes in iron-regulatory gene expression occur in human cell culture models of Parkinson's disease. *Neurochem. Int.* **59,** 73–80
35. Jerjes, W., Upile, T., Hamdoon, Z., Alexander Mosse, C., Morcos, M., and Hopper, C. (2011) Photodynamic therapy outcome for T1/T2 N0 oral squamous cell carcinoma. *Lasers Surg. Med.* **43,** 463–469
36. Tan, I. B., Dolivet, G., Ceruse, P., Vander Poorten, V., Roest, G., and Rauschning, W. (2010) Temoporfin-mediated photodynamic therapy in patients with advanced, incurable head and neck cancer: A multicenter study. *Head Neck* **32,** 1597–1604